AUTHOR MANUSCRIPT | PUBLICATION & REUSE INFORMATION

Contact-Triggered Sequential Grasping With an HSA-Driven Underactuated Gripper for Delicate Produce

Xiaoqian Zhang, Mario Baggetta, Cristina Piazza, and Giovanni Berselli

IEEE/ASME Transactions on Mechatronics, vol. 31, no. 4, pp. 4828-4836, 2026.

Published version: https://doi.org/10.1109/TMECH.2026.3696423

This is the author-prepared manuscript, provided on the author's personal website for individual scholarly use. Please cite the published version using the DOI above.

© 2026 IEEE. Personal use of this material is permitted. Permission from IEEE must be obtained for all other uses, in any current or future media, including reprinting/republishing this material for advertising or promotional purposes, creating new collective works, for resale or redistribution to servers or lists, or reuse of any copyrighted component of this work in other works.

Presentation preparation: publication and copyright information added. A duplicated opening sentence in the manuscript abstract was corrected to match the published abstract. The original local source file is preserved. The publisher version remains the version of record.

Contact-Triggered Sequential Grasping with an HSA-Driven Underactuated Gripper for Delicate Produce

Xiaoqian Zhang, Mario Baggetta, Cristina Piazza, and Giovanni Berselli

Abstract - A main challenge in agri-tech lies in robotic handling and harvesting of delicate produce.

Traditional end-effectors struggle to balance grip stability, adaptability to irregular items, and bruise mitigation. In this work, a soft gripper based on handed shearing auxetic (HSA) structures is presented. The gripper adopts a dual-module architecture composed of a Target Tracking System (TTS) and a Pinch-Grasp System (PGS). A passive tendon-driven differential shifts the grasping center after early contact, compensating for target misalignment without active sensors. The PGS employs HSA units to achieve transition from parallel pinching to bending-based enclosure through contact-induced torque redirection. Both modules share a single actuator and preserve a minimal transmission architecture. Finite element simulations and response surface exploration identify key stiffness and geometric parameters, guiding the rigid-body synthesis of the TTS and actuator selection. Experiments on objects with varying offsets, diameters, and pull-out conditions, including pinch-only and side-entry tests, assess the ability to self-center, pinch, and enclose without additional control layers. The results indicate that HSA actuation combined with passive differentials can provide a compact mechanism-level solution for produce-oriented grasping under representative benchtop conditions.

***Index Terms*—Soft grippers, under actuation, handed shearing auxetic actuator, passive differential, contact–induced mode switching**

I. Introduction

AUTOMATION in fresh produce handling and harvesting places demanding requirements on end-effectors. Delicate fruit and irregular agricultural items exhibit limited tolerance to concentrated stresses, requiring tools that combine grip stability with minimal surface damage [1]–[5]. Conventional rigid grippers often struggle in these scenarios, as their performance is highly dependent on precise positioning. The limited contact areas through which they interact with the object can generate concentrated and non-uniform loads on the fruit surface [6], [7], increasing the risk of bruising. By contrast, compliant mechanisms can distribute contact pressure more gradually and tolerate geometric uncertainty and surface irregularities more effectively [8]–[10].

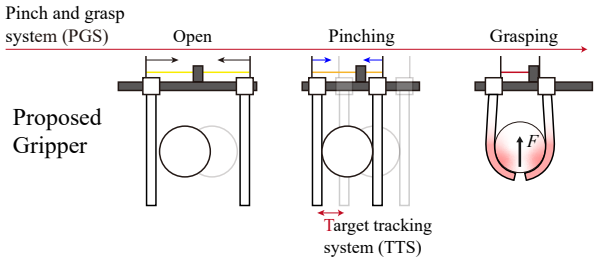


Fig. 1. Working principle of the Pinch-Grasp System (PGS) and Target Tracking System (TTS).

These advantages are accompanied by important trade-offs. Fully compliant fingers often provide limited directional support and reduced usable gripping forces in agricultural applications. Fin-Ray inspired structures illustrate this limitation well, since their passive adaptation may constrain motion guidance and leave the fingers susceptible to pull-out when handling heavier produce [6], [11]. Tendon-driven underactuation partially addresses these issues by redistributing actuation travel, so that non-contacting fingers can continue to move and passively share forces during grasp formation [12]–[16]. Related studies have also explored contact-triggered reconfiguration, where contact at one location passively redirects the remaining actuation travel to other parts of the system, enabling sequential behaviors such as pinching and enclosure [17], [18]. Another important challenge concerns grip integrity under external disturbances and lifting forces, as harvesting-oriented studies report apple detachment forces up to approximately 40 N [19]; accordingly, soft coverings, geometric reconfiguration, and tendon-routing strategies have

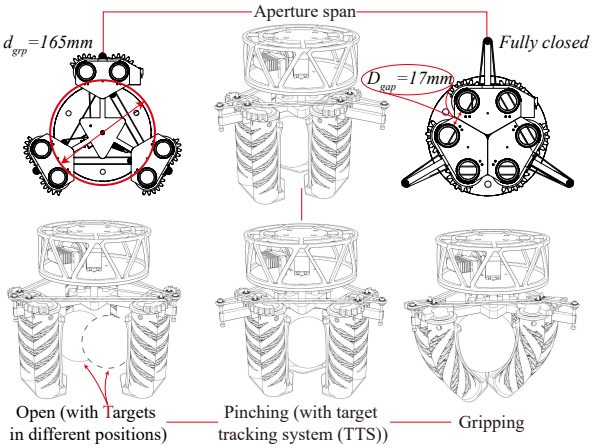


Fig. 2. CAD model of the gripper under different target positions and grasping conditions.

This work was supported by FISA-2023-00358, Horizon Europe Research and Innovation Programme INTELLIMAN (G.A. 101070136), AI-AGRI-HAND and euROBIN (G.A. 101070596).

X. Zhang is affiliated with both the Department of Mechanical Engineering, University of Genoa, 16145 Genoa, Italy, and the TUM School of Computation, Information and Technology and the Munich Institute of Robotics and Machine Intelligence (MIRMI), Technical University of Munich, 80333 Munich, Germany (e-mail: xiaoqian.zhang@edu.unige.it).

M. Baggetta and G. Berselli are with the Department of Mechanical Engineering, University of Genoa, 16145 Genoa, Italy.

C. Piazza is with the TUM School of Computation, Information and Technology and the Munich Institute of Robotics and Machine Intelligence (MIRMI), Technical University of Munich, 80333 Munich, Germany.

Corresponding authors: Giovanni Berselli (giovanni.berselli@unige.it) and Cristina Piazza (cristina.piazza@tum.de).

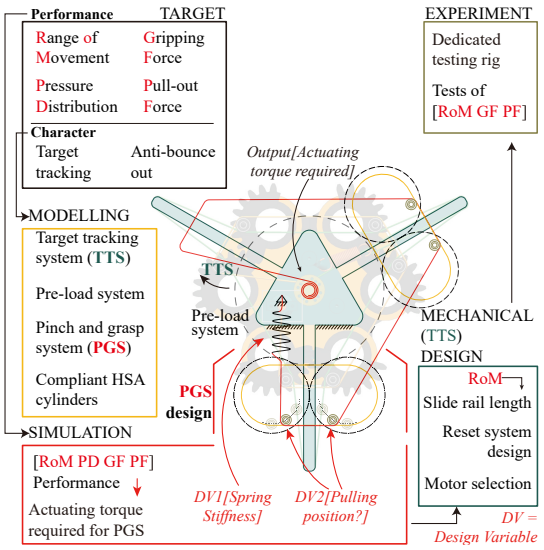


Fig. 3. Methodology and roadmap of the proposed gripper.

been investigated to improve pull-out resistance and load sharing [20]–[23].

Handed-shearing auxetic (HSA) structures provide a continuous, architected medium capable of producing coupled twisting and extension under torque input [24], [25]. Their mechanical response can be tuned through geometric design alone, and electrically driven variants have demonstrated compact integration without the need for pumps or external hardware [26], [27]. These characteristics make HSAs attractive candidates for end effectors where both compliance and directed deformation are needed.

Building on these observations, this work presents a gripper composed of two cooperative subsystems: a target tracking system (TTS) and a pinch-grasp system (PGS). The TTS passively redistributes actuation travel among three fingers after early contact, shifting the effective grasping center toward the target center and facilitating the handling of eccentrically positioned objects. Compared with prior HSA-based grippers mainly focused on electrically driven compliant grasping, the proposed system combines HSA-enabled enclosure with passive target tracking and contact-triggered sequential grasping. The PGS exploits contact-induced rotation at the HSA end cap to transition from an initial planar pinch to a curved enclosure, thereby improving pull-out resistance while maintaining gentle surface contact.

Both subsystems are driven by a single motor and rely on a minimal linkage architecture. Their interaction is summarized in Fig. 1, which illustrates the sequence from approach to full enclosure. An overview of the proposed methodology is provided in Fig. 3, including functional requirements, modeling steps, structural optimization, and prototype validation. Experimental evaluations involving eccentric targets, object size variations, and pull-out conditions assess the proposed concept under representative benchtop conditions.

II. Methods

Since all three fingers share identical geometry and transmission, this section introduces the overall assembly and grasping sequence, then the simulation-based design of the

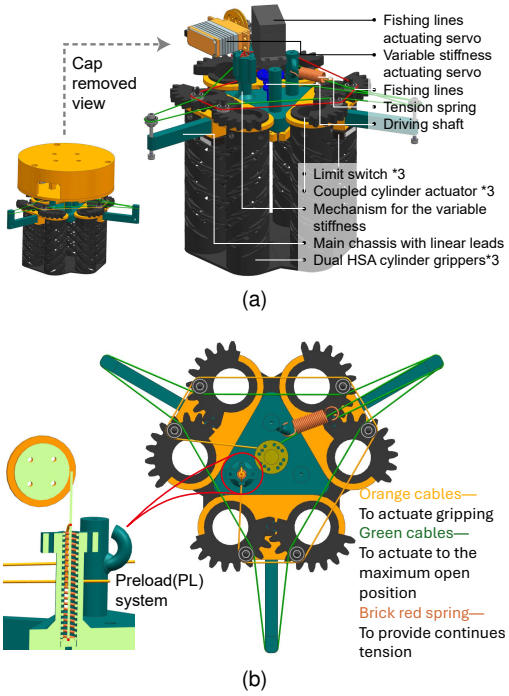


Fig. 4. Overall assembly: (a) perspective view; (b) top view of cable driven underactuated mechanism.

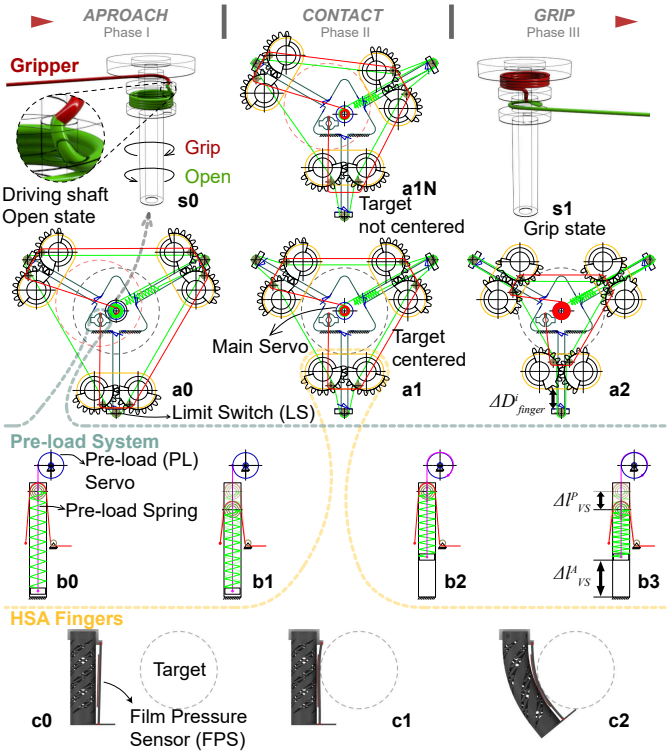
PGS, and finally the simplified mechanical drive analysis used for actuator sizing and range definition. The complete assembly is shown in Fig. 4. The main drive shaft winds two tendon branches, which serve the closing and opening functions, respectively. Because the two branches wrap around the shaft with different numbers of turns, the available tendon travel differs between closing and opening motions. A preloaded spring, highlighted in brick red in Fig. 4, maintains tension in the tendons and prevents slack, which could otherwise lead to unintended object release. The total prototype weight is approximately 757 g, of which the three HSA cylinders account for about 120 g.

A. Grasping Sequence and Control Logic

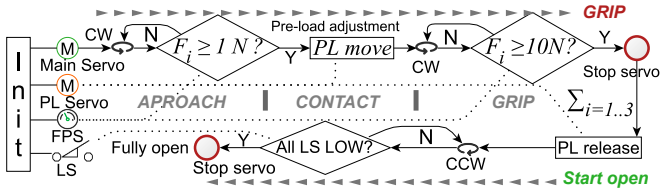
The operating sequence mechanism is in Fig. 5a, and its associated control logic is summarized in Fig. 5b. Limit switches (LS) at the end of each linear guide define the fully open configuration. In this state, all fingers rest at their outermost positions along the rails, and the preload (PL) subsystem is set to its minimum preload, ensuring that the initial interaction with the object remains compliant and tolerant to contact uncertainties.

From the initial pose, the main shaft rotates in the closing direction. In the physical implementation, the "red" closing tendon and the "green" opening tendon are two ends of the same line. As the shaft winds the closing side, it releases the opening side at nearly the same rate. With the inner mechanical stops on the main chassis taken as reference, the distance between the i-th finger and its inner stop is defined as $\Delta D^i_{\text{finger}}$. The sum $\sum_{i=1}^{3} \Delta D^i_{\text{finger}}$ decreases as the closing tendon is pulled, corresponding to inward sliding of the fingers along the guides.

Continued shaft rotation drives the fingers toward the object. The target may be near the geometric center of the gripper,



(a) Flow chart for grasping mechanism behavior



(b) Control flow chart for grasping behavior

Fig. 5. Mechanism and control flow charts for grasping behavior.

but in practice it is often offset. As soon as one finger touches the object, the corresponding carriage is blocked on its rail. Due to the underactuated tendon routing, the remaining fingers continue to move inward and adapt to the actual target position, while the first-contact finger stays in place.

Each finger is equipped with a film pressure sensor (FPS). When all three fingertips have reached the object and the sum of their readings exceeds a prescribed threshold, the system interprets this as a transition into the pinch phase. In the experiments, this condition was set as

$$\sum_{i=1}^{3} F_i \geq 1 \text{ N},$$

where F_i is the normal force measured by the i-th sensor. At this point, the PL subsystem is activated. The PL adjusting tendon is pulled by a displacement $\Delta l_{\mathrm{PL}}^{A}$, and the preload of the internal springs increases. This adjustment raises the maximum pull-out resistance while keeping the contact forces within acceptable limits.

The main shaft then continues to rotate in the same direction. Because the object blocks further sliding on the rails, the relative position of each finger along its guide remains almost unchanged. In the default grasping configuration, the additional tendon travel is converted by the handed shearing auxetic (HSA) structure into bending at the distal end. The fingers curl around the object and move from a pinch configuration to a more enveloping grasp. The increased tendon tension in this phase is transmitted to the PL module, so that the springs in the double pulley arrangement are stretched by approximately $2\Delta l_{\mathrm{PL}}^{A}$. In parallel, the fingertip force readings continue to grow. When the average force per finger reaches a higher threshold,

$$\bar{F} = \frac{1}{3}\sum_{i=1}^{3} F_i \approx 10 \text{ N},$$

the grasp is regarded as successful for the given test conditions, and the main servo stops.

Reopening follows the reverse sequence. The PL servo first returns the PL setting to its minimum value. The drive shaft is then rotated counterclockwise so that the opening tendon pulls the fingers outward along their rails. Due to the underactuated topology, fingers that have already reached the LS position remain blocked, and the residual tendon travel is redistributed to the remaining fingers. Once all three LS switches have been triggered, the system has returned to the initial open pose, and the main servo is stopped again.

B. Simulation Based Design of the PGS

The pinch and grasp system (PGS) relies on three HSA-based fingers, each formed by a continuous flexible body rather than a chain of discrete rigid links. To evaluate the influence of design parameters on performance, a finite element model of a single finger was developed in Ansys 2022 R1. The simulation focuses on the PGS alone and explores the relationship between selected design variables and several performance indicators. The main components of the model, including the input variables, boundary conditions, contact pairs, material assignment, and output probes, are summarized in Fig. 6. The equivalent tendon loading is represented by concentrated spring forces to reduce computational cost.

Two design variables are investigated. The first is the stiffness of the spring in the PL module, used to adjust the preload range in the physical prototype. This preload influences the passive compliance of the finger during gripping and pull-out. A smaller preload leads to a more compliant response and a more uniform force profile during extraction, whereas higher preload results in a sharper force increase near the end of the pull-out. The adjustment range enabled by this spring therefore defines the lower bound of the achievable compliance under load.

The second design variable is the initial angular position of the driven end cap relative to the fixed frame. In the model, this position is defined as an angle around the HSA end face. Angles pointing outward along the HSA perimeter are treated as negative, and angles pointing inward are treated as positive. This starting angle controls both the effective stroke and the evolution of mechanical advantage during actuation. A large positive angle gives a short motion range with an earlier transition to high force, whereas more negative angles provide a wider stroke but a slower force build-up. Since the

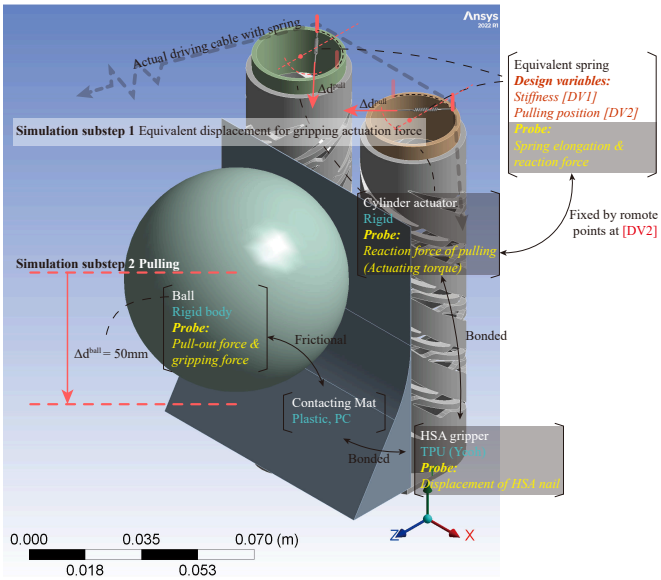


Fig. 6. Simulation setup for one finger of the PGS system. Red lines and texts stand for the input conditions and design variables, blue texts stand for the properties assigned for the objects in simulation, yellow texts stand for the output parameters expected.

HSA segment requires increasing drive force as it bends, the cap angle must be selected so that the available torque remains compatible with the HSA demand over the full motion range.

Material properties and contact definitions follow the physical prototype and the expected interaction between HSA, springs, fingernail, and the test object. The motion is divided into two substeps that mimic the experimental procedure: the first corresponds to approaching and forming the grasp, and the second to pulling the object out of the grasp. To reduce the computational cost associated with explicitly modeling the full cable path, the tendon action is represented by direct spring elements acting on the drive point of the end cap, oriented along the actual tendon direction, for parameter selection and local performance comparison within the PGS.

A design of experiments (DoE) study was carried out on this model, and the results are summarized in Fig. 7. The analysis monitors three main outputs: maximum gripping force, maximum pull-out force, and fingertip displacement. Panels (a), (c), and (e) in Fig. 7 show how these outputs vary with the initial cap angle and spring stiffness. In the range explored, the optimal initial cap angle for both force and displacement is consistently around $-10°$, largely independent of the chosen spring stiffness, and was therefore selected as the nominal setting for the prototype.

With the initial angle fixed at $-10°$, the maps in Fig. 7(b), (d), and (f) are used to select a suitable spring stiffness. In the physical layout, the relaxed spring length is constrained to approximately 50 mm. Under these constraints, a stiffness of about 1 N/mm yields a maximum compression of 5.2 mm in the simplified model. When mapped to the full assembly, which is equivalent to six springs acting in parallel, this corresponds to a total compression of roughly 31.2 mm, compatible with the mechanical limits of the housing.

For the selected design, the maximum spring reaction force sets the minimum drive force required for a single HSA

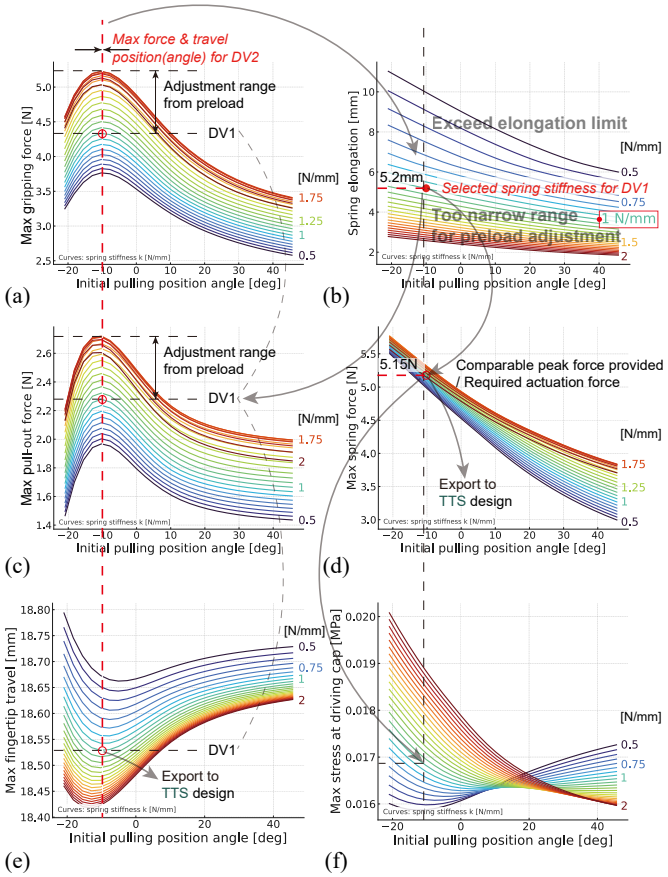


Fig. 7. Design variable selection and partial output acquisition, i.e., actuating torque required and adjustment range from preload, based on a simulation-based design of experiments (DoE).

module in the simplified model of the PGS. The simulations indicate that this force remains close to 5.15 N across the range of spring stiffness values considered, which facilitates actuator sizing. This value is later used in the mechanical analysis of the target tracking system. This value refers to a simplified single-cylinder design model and is not directly comparable to the experimental peak pull-out force of the assembled gripper. The structural checks in Fig. 7(f) confirm that the peak stresses in the HSA body remain below the material strength, indicating that the selected parameters do not compromise durability. The pull-out behavior predicted by the model is illustrated in Fig. 7(c). For the selected configuration, the maximum pull-out force over the trajectory in the simplified single-finger model used for design comparison lies between 2.3 and 2.7 N, depending on the chosen preload. The fingertip displacement, shown in Fig. 7(e), is approximately 18.5 mm and is used later as a reference when designing the motion range of the target

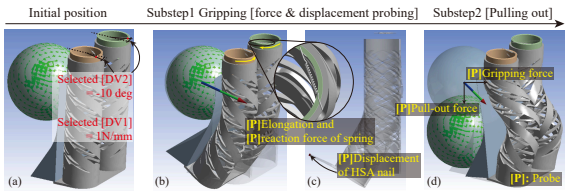


Fig. 8. Simulation result under the selected design variables.

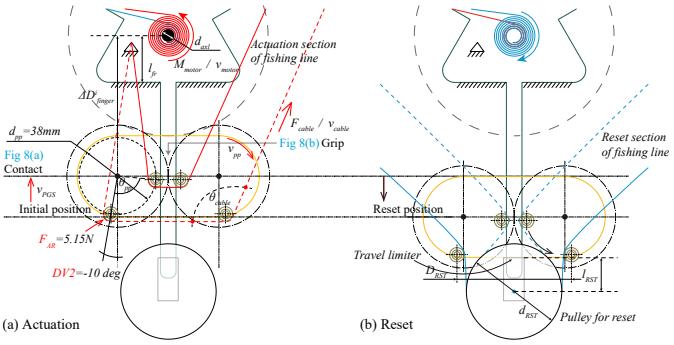


Fig. 9. Drive mechanism used for grasping and resetting: (a) closing layout, (b) reset layout.

tracking system.

Figure 8 collects representative snapshots from the simulation under the chosen design variables. The sequence is consistent with the experimental grasping process, from approach through initial pinch and bending to pull-out.

C. Mechanical Design of the Drive Mechanism

The underactuated layout of the gripper operates on two levels. First, the three fingers share a common tendon path while sliding along their individual rails. Second, within each finger and rail assembly, an additional underactuated stage is implemented. The structural design of this stage governs the sequence of the approach and grasp phases in the pinch and grasp system (PGS). The same mechanism is also used during reopening and reset.

Figure 9 presents a simplified view of the drive mechanism. In the closing path, six tendon segments leave the main shaft, pass around guiding pulleys, and then act on the fingers in directions that are not perfectly aligned with the desired gripping force direction. Denoting the direction of the resultant gripping force as the F_{AR} axis, the i-th tendon leaves its last pulley at an angle θ_i with respect to this axis. In the present design, these angles are approximately

$$\theta_i = \{80^\circ,\ 120^\circ,\ 120^\circ,\ 120^\circ,\ 120^\circ,\ 70^\circ\}.$$

Each tendon segment carries a tension $F_{\text{cable},i}$. Its contribution along the F_{AR} axis is $F_{\text{cable},i}\cos\theta_i$, so the total gripping force can be written as

$$F_{\text{AR}} = \sum_{i=1}^{6} F_{\text{cable},i}\ \cos\theta_i. \tag{1}$$

To simplify the relation between tendon tension and gripping force, an equivalent angle θ_{eq} is introduced. Under the assumption that all tendon segments carry approximately the same tension F_{cable}, the expression becomes

$$F_{\text{AR}} \approx F_{\text{cable}}\ \cos\theta_{\text{eq}}, \tag{2}$$

and the required tendon tension can be estimated as

$$F_{\text{cable}} \approx \frac{F_{\text{AR}}}{\cos\theta_{\text{eq}}}. \tag{3}$$

This relation provides a simplified estimate of the average tendon load associated with a target gripping force. This projection-based relation is used here as a pre-contact sizing approximation. After object contact, tendon directions and load sharing evolve with finger deformation and contact constraints.

Once the required tendon tension F_{cable} is known, the minimum torque and speed for the motor can be evaluated. For a shaft with diameter $d_{\text{axl}} = 8$ mm, the minimum torque at the motor output is

$$M_{\text{motor,min}} = F_{\text{cable}}\,\frac{d_{\text{axl}}}{2}. \tag{4}$$

The linear speed of the tendon is related to the rotational speed of the shaft by

$$v_{\text{cable}} = \omega_{\text{motor}} r = v_{\text{motor}}\,\pi d_{\text{axl}}, \tag{5}$$

where $r = d_{\text{axl}}/2$, ω_{motor} is the angular speed, and v_{motor} is the rotational speed in revolutions per unit time. Solving for v_{motor} gives

$$v_{\text{motor}} = \frac{v_{\text{cable}}}{\pi d_{\text{axl}}}, \tag{6}$$

which directly links the shaft speed to the desired closing speed of the tendons. Equations (4) and (6) together provide a first-order basis for motor selection once a target gripping force and closing time are specified, with friction in the tendons, pulleys, and guides neglected in this estimate. In the prototype, the main shaft was actuated by a 360° continuous-rotation MG996-class servo with a rated torque of approximately 20 kgf · cm (≈ 1.96 N · m), which is well above the calculated minimum requirement.

The PGS also incorporates a fingertip sliding mechanism to accommodate objects of different sizes. The intended application is medium-sized apple/pear-like fruit with diameters of 60 to 90 mm, evaluated using a 10 N/finger final contact level and a ~ 40 N pull-based retention reference. To support this diameter range, the closing stroke of the gripper should accommodate the expected variation in object diameter.

Each fingertip can slide passively along its guide by a displacement $\Delta D_{\text{finger}} = 18.5$ mm. This travel is defined by the distance l_{fr} between the mechanical stop on the base and the limit piece on the fingertip carriage. When one fingertip touches the object first, its motion along the rail stops, but the tendon tension continues to increase and eventually overcomes the static friction at the limit interface, causing the fingertip carriage to slide along the guide. The combined remaining sliding travel of the two opposing fingers is

$$\Delta D_{\text{total}} = 2\,\Delta D_{\text{finger}} = 37\ \text{mm}. \tag{7}$$

For the target objects, the diameter variation is approximately 30 mm, denoted ΔD_{object}. The design satisfies

$$\Delta D_{\text{total}} \geq \Delta D_{\text{object}}, \tag{8}$$

thereby ensuring that the mechanism can adapt to objects in the 60 to 90 mm range without losing symmetry or contact quality. From the CAD model, the maximum gripper aperture is approximately $d_{grp} = 165$ mm, while the nearly closed configuration leaves a residual finger gap of about $D_{gap} = 17$ mm.

The reset path of the mechanism uses a separate tendon segment with a spring to enable passive self-centering behavior.

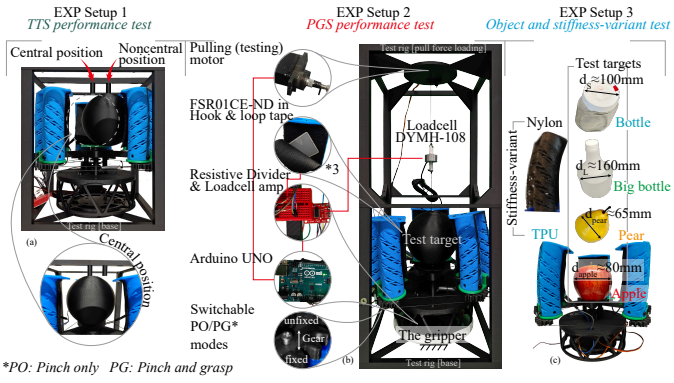


Fig. 10. Experimental setups for testing the TTS, PGS, a nylon-based stiffness variant and real-object grasping. Setup 2 includes a switchable gear-fixation mechanism for comparing pinch-only (PO) and pinch-and-grasp (PG) modes.

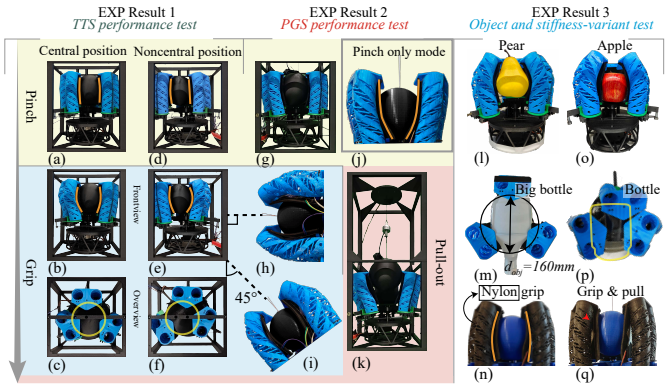


Fig. 11. Key stages of the gripper during the experiments, including centered and off-centered grasping, side-entry tests, pinch-only mode, pull-out behavior, representative real-object grasps, and a nylon-based stiffness variant.

The initial tension is set high enough to keep the tendons taut and to draw the pulleys and carriages back toward the center once the main drive motor is released. This enables passive reset without additional sensing or active control beyond releasing the main drive.

III. Experiments

The gripper integrates a target tracking system (TTS) and a pinch and grasp system (PGS), both driven by a single actuator and coordinated through the control logic in Fig. 5a. To evaluate subsystem performance and grasping behavior in representative scenarios, dedicated experimental fixtures were developed, as shown in Fig. 10. The lower frame constrains the gripper at its mounting interface and supports interchangeable targets at prescribed positions, while an upper frame is added when pull-out loading is required.

Three experimental setups were used. In setup 1, a suspended spherical target was used to evaluate the passive target-tracking capability of the TTS under centered and intentionally off-centered conditions. The influence of tendon preload was examined by varying the preload displacement Δx of the PL spring. Setup 2 quantified the pull-out performance of the PGS using a controlled extraction rig, with pull-out force measured by an in-line load cell. Besides the default pinch-and-grasp (PG) mode, a pinch-only (PO) mode was implemented by fixing one gear in each finger to the corresponding TTS carriage with a screw, thereby disabling HSA bending while preserving translational pinching motion. Additional tests were also conducted at side-entry orientations of 45° and 90° under the same loading protocol. Setup 3 evaluated representative real objects using the same grasp-pull protocol, focusing on enclosure formation, force sharing, and retention under subsequent pull-out loading.

Both qualitative and quantitative evaluations were conducted. Qualitative snapshots illustrate the grasping sequence, side-entry behavior, pinch-only configuration, and enclosure behavior (Fig. 11), while quantitative measurements report gripping and pull-out forces (Fig. 12–Fig. 14). Contact forces were monitored using film pressure sensors mounted on the inner finger surfaces. All sensors and actuators were controlled via an Arduino UNO, with data logged on a host computer.

For each quantitative condition, 20 grasping cycles were executed to account for stabilization of the HSA response, and five trials were extracted for analysis. The reported results are presented as mean curves with error bands. Side-entry peak pull-out values are summarized in Table I. For the real-object tests, visible damage was assessed by post-grasp visual inspection.

IV. Results

Figure 11 summarizes the qualitative grasping sequences observed across the three experimental setups. Quantitative force results are reported in Fig. 12–Fig. 14.

In setup 1 with a centered spherical target, all three fingers establish contact nearly simultaneously and progress toward enclosure, resulting in balanced force profiles. Peak gripping forces approached the prescribed 10 N/finger level. Increasing the preload leads to a steeper and more repeatable force rise, while lower preload produces a more compliant response with higher variability. In off-centered tests, the final grasp consistently recenters with respect to the target. An additional constrained-TTS comparison for this setup is provided in the supplementary material. Two fingers may contact earlier, while the remaining finger continues to move until full engagement is achieved.

Setup 2 evaluates pull-out behavior relative to the intended pull-based retention target of about 40 N. In the default PG mode, the maximum pull-out force reaches approximately 45 N for an 80 mm spherical target in the assembled three-finger gripper. The additional 45° and 90° side-entry tests yield comparable mean peak pull-out forces, approximately 46 N and 47 N, respectively. No evident gravity-induced degradation in grasp formation or pull-out resistance was observed across the tested approach orientations. The force evolution indicates a gradual release without abrupt jump-out, reflecting the combined contribution of enclosure and fingernail interaction. In the PO mode, the front-view contact geometry becomes V-shaped, and the corresponding pull-out curve exhibits a pronounced force valley before nail engagement. Under the same gripping threshold, the maximum pull-out force remains around 25 N, substantially lower than in PG mode. For the 80 mm spherical target, increasing the preload from 2 N (Δx = 1 mm) to 5 N and then to the fully compressed spring condition (Δx = 11 mm) increased the peak gripping force from 8.5 N to 9.2 N and 10 N, and the corresponding peak

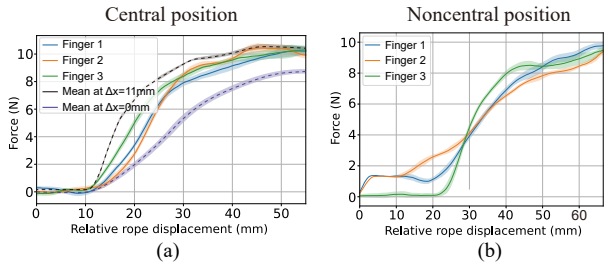


Fig. 12. Gripping force results for experimental setup 1 (TTS), showing the influence of target offset and preload setting.

TABLE I
BENCHMARK SUMMARY OF THE PROPOSED GRIPPER AND REPRESENTATIVE HARVESTING-ORIENTED GRIPPERS.

System	Object	Mode	Cond.	Main result
Proposed gripper	80 mm sphere	PG	0°/45°/90°	Peak pull-out force ≈ 45/46/47 N
	80 mm sphere	PO	0°	Peak pull-out force ≈ 25 N
	Pear / apple / bottle / large bottle	PG	65–160 mm tested	Peak pull-out force: 42 / 47 / 45 / 35 N; no visible damage
Chen et al. (2022)	Apple	Pull	65–95 mm	Detachment force: 8.88–39.6 N; 80% picking success; 0% fruit skin damage
Wang et al. (2023)	Apple	Twist-pull	Apple harvesting	Detachment / damage / harvesting rate: 75.6% / 4.55% / 70.77%
Visentin et al. (2023)	Strawberry	Pull	Small fruits	Force range: 0–4 N; 82% correct picking rate

pull-out force from 39 N to 42 N and 45 N. An additional nylon-printed HSA variant reached a substantially higher peak pull-out force of about 98.4 N, but exhibited visibly reduced conformability and a marked increase in average finger force during extraction before nail engagement, as highlighted in Fig. 11(q) and indicated by the dashed curve in Fig. 13(a). Compared with the TPU fingers, the contact force no longer remained close to the prescribed gripping level during the later stages of extraction.

In setup 3, representative grasps on real objects illustrate the intended underactuated behavior. Symmetric objects lead to balanced three-finger enclosures, while asymmetric early contact on horizontally placed objects does not prevent completion of the grasping sequence. In all cases, non-contacting fingers continue to move and complete the enclosure, improving force sharing while limiting local overload. Fig. 14 reports the corresponding gripping-force profiles, while the pull-out results are summarized in Table I. No visible surface damage was observed on the tested objects under post-grasp visual inspection. Grip success rate was 100% for all tested objects, and retention success rates were 100%, 100%, 95%, and 75% for the pear, apple, bottle, and large bottle, respectively. Based on the CAD-defined lower bound and the tested objects, the practical retainable size range was approximately 17–160 mm. The upper bound was inferred from the large-bottle grasp in Fig. 11(m), with $d_{obj} = 160$ mm, and was taken as the approximate upper practical grasp limit under the current finger geometry.

V. DISCUSSION AND FUTURE WORK

For both centered and off-centered targets, the three fingers converge toward a common enclosure, and the measured

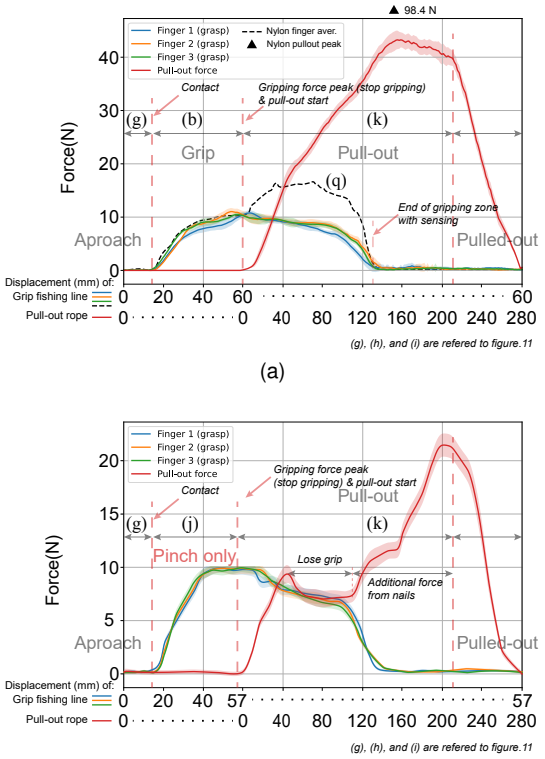


Fig. 13. Setup 2 force results in PG (a) and PO (b) modes. The dashed curve denotes the nylon-printed HSA variant; side-entry peaks are summarized in Table I.

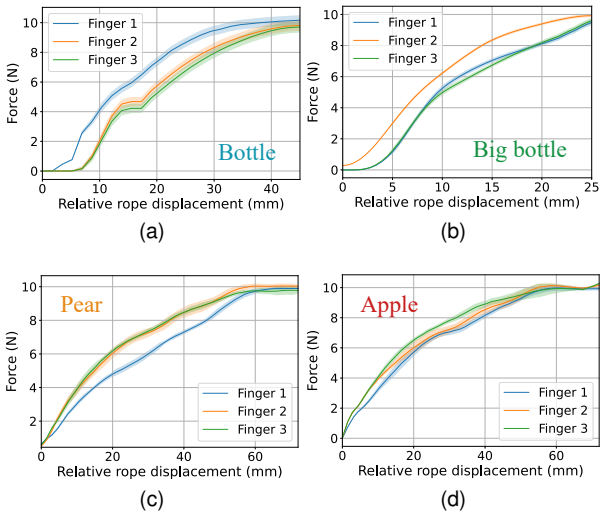


Fig. 14. Gripping force results for experimental setup 3 on representative real objects, including a bottle, a large bottle, a pear, and an apple.

contact forces reach comparable levels once the pinch-to-grasp transition is completed. In pull-out tests with an 80 mm spherical target, the resistance to extraction increases smoothly and reaches a peak of approximately 45 N before release, without abrupt force drops or sudden jump-out behavior.

The range of objects successfully grasped in the experiments spans object sizes from roughly 65 mm to 160 mm. This range reflects the tested objects and the combined contribution of the sliding-based target tracking mechanism and the compliant enclosure provided by the HSA-driven fingers. Rather than relying on precise initial alignment, the gripper adapts its con-

figuration after early contact, allowing the remaining fingers to continue their motion until a mechanically balanced grasp is formed. The comparison with the nylon-printed HSA variant suggests a trade-off between retention and compliant load redistribution: increasing structural stiffness can substantially raise pull-out resistance, but at the cost of reduced conformability and a less controlled increase in contact force during extraction.

The influence of tendon preload is primarily observed during the transient phase of force development. Lower preload settings lead to a more gradual and compliant force increase, accompanied by larger trial-to-trial variability, whereas higher preload produces a steeper initial rise with improved repeatability. In all cases, the maximum gripping force remains comparable, indicating that the upper force level is governed mainly by the actuation capability of the HSA-based PGS rather than by the preload level itself.

From a design perspective, the current prototype demonstrates the feasibility of integrating passive target tracking and contact-triggered enclosure within a single-actuator architecture. The overall size of the mechanism is still influenced by the dual-HSA finger layout and the associated sliding rails. Future work will therefore explore more compact finger architectures, such as single-HSA designs constrained by rigid elements, while maintaining the same functional sequence. The present validation focuses on pull-based retention and grasp stability. A wrist-enabled detachment strategy introducing combined torsion–tension loading will be considered in future work. Quantitative bruise assessment also remains an important direction for future study. The present experiments do not isolate shear slip resistance as a separate interface-level metric; instead, retention was evaluated at the system level through pull-out tests. Under the same 80 mm spherical target and pulling protocol, the PG mode maintained retention up to approximately 45 N, whereas the PO mode showed an early loss-of-grip region and a lower peak value of about 25 N, indicating that the enclosing grasp improves resistance to tangential slip during extraction.

The results support a feasible pull-based mechanism-level approach for produce-oriented handling under representative benchtop conditions, with reduced dependence on precise positioning and without additional sensing or control layers.

REFERENCES

[1] Q. Wang *et al.*, "Towards damage-less robotic fragile fruit grasping: A systematic review on system design, end effector, and visual and tactile feedback," *Journal of Field Robotics*, vol. 42, no. 8, pp. 4521–4543, 2025.

[2] X. Wang, H. Kang, H. Zhou, W. Au, M. Y. Wang, and C. Chen, "Development and evaluation of a robust soft robotic gripper for apple harvesting," *Computers and Electronics in Agriculture*, vol. 204, p. 107552, 2023.

[3] D. Zhang, W. Zhang, H. Yang, and H. Yang, "Application of soft grippers in the field of agricultural harvesting: A review," *Machines*, vol. 13, no. 1, p. 55, 2025.

[4] Y. Jiang and J. Mohammadpour Velni, "A soft robotic gripper for crop harvesting: Prototyping, imaging, and model-based control," *AgriEngineering*, vol. 7, no. 11, p. 378, 2025.

[5] K. Zhang, K. Lammers, P. Chu, Z. Li, and R. Lu, "An automated apple harvesting robot—from system design to field evaluation," *Journal of Field Robotics*, vol. 41, no. 7, pp. 2384–2400, 2024.

[6] J. Shintake, V. Cacucciolo, D. Floreano, and H. Shea, "Soft robotic grippers," *Advanced Materials*, vol. 30, no. 29, p. 1707035, 2018.

[7] J. Wang, C. Wang, and J. Wu, "Characterization of contact pressure distribution and bruising prediction of apple under compression loading," *Processes*, vol. 12, no. 3, p. 543, 2024.

[8] J. F. Elfferich, D. Dodou, and C. D. Santina, "Soft robotic grippers for crop handling or harvesting: A review," *IEEE Access*, vol. 10, pp. 75 428–75 443, 2022.

[9] F. Visentin, F. Castellini, and R. Muradore, "A soft, sensorized gripper for delicate harvesting of small fruits," *Computers and Electronics in Agriculture*, vol. 213, p. 108202, 2023.

[10] S. Dontu *et al.*, "Applications of a vacuum-actuated multi-material hybrid soft gripper: lessons learnt from robosoft manipulation challenge," *Frontiers in Robotics and AI*, vol. 11, p. 1356692, 2024.

[11] S. Terrile, M. Argüelles, and A. Barrientos, "Comparison of different technologies for soft robotics grippers," *Sensors*, vol. 21, no. 9, p. 3253, 2021.

[12] M. Manti, T. Hassan, G. Passetti, N. d'Elia, M. Cianchetti, and C. Laschi, "An under-actuated and adaptable soft robotic gripper," in *Lecture Notes in Computer Science*. Springer International Publishing, 2015, pp. 64–74.

[13] M. Bluiminck and W. Roozing, "An underactuated tendon-driven gripper with variable stiffness for deformable agri-food objects," in *2023 IEEE 19th International Conference on Automation Science and Engineering (CASE)*, 2023, pp. 1–8.

[14] V. Burini, S. Logozzo, and M. C. Valigi, "A new smart gripper with soft fingers and integrated force sensors for adaptive robotic tasks," *Robotics and Autonomous Systems*, vol. 195, p. 105218, 2026.

[15] K. Dwarshuis, J. De Jong, and D. Brouwer, "Design of an underactuated, flexure-based gripper, actuated through a push–pull flexure," *Journal of Mechanisms and Robotics*, vol. 17, no. 6, p. 061009, 2025.

[16] X. Zhao, L. He, Y. Li, J. Chen, and C. Wu, "Kinetostatic modeling of clamping force in a tendon-driven soft robotic gripper for tea shoot plucking," *Computers and Electronics in Agriculture*, vol. 236, p. 110441, 2025.

[17] T. Nishimura, K. Mizushima, Y. Suzuki, T. Tsuji, and T. Watanabe, "Variable-grasping-mode underactuated soft gripper with environmental contact-based operation," *IEEE Robotics and Automation Letters*, vol. 2, no. 2, pp. 1164–1171, 2017.

[18] S. Ansari, M. K. Gohil, and B. Bhattacharya, "A novel approach to tomato harvesting using a hybrid gripper with semantic segmentation and keypoint detection," 2024, arXiv:2412.16755.

[19] K. Chen *et al.*, "A soft gripper design for apple harvesting with force feedback and fruit slip detection," *Agriculture*, vol. 12, no. 11, 2022.

[20] M. Baggetta, O. Pennacchio, S. Pirozzi, and G. Berselli, "A reconfigurable four-finger gripper for versatile application in the agri-food industry," *IEEE/ASME Transactions on Mechatronics*, vol. 30, no. 4, pp. 2999–3007, 2025.

[21] S. M. Kargar and G. Berselli, "Tricom gripper–part i: Mechanical design and synthesis of a 3-finger compliant monolithic gripper," in *2024 20th IEEE/ASME International Conference on Mechatronic and Embedded Systems and Applications (MESA)*, 2024, pp. 1–6.

[22] S. M. Kargar and G. Berselli, "Tricom gripper–part ii: Soft pad integration and virtual prototyping for delicate object handling," in *2024 20th IEEE/ASME International Conference on Mechatronic and Embedded Systems and Applications (MESA)*, 2024, pp. 1–6.

[23] M. Baggetta, G. Hao, and G. Berselli, "Design and virtual prototyping of a constant force gripper for food handling and harvesting," in *Volume 2: 43rd Computers and Information in Engineering Conference (CIE)*, 2023, p. V002T02A024.

[24] L. Chin, J. Lipton, R. MacCurdy, J. Romanishin, C. Sharma, and D. Rus, "Compliant electric actuators based on handed shearing auxetics," in *2018 IEEE International Conference on Soft Robotics (RoboSoft)*, 2018, pp. 100–107.

[25] R. L. Truby, L. Chin, and D. Rus, "A recipe for electrically-driven soft robots via 3d printed handed shearing auxetics," *IEEE Robotics and Automation Letters*, vol. 6, no. 2, pp. 795–802, 2021.

[26] I. Good, T. Brown-Moore, A. Patil, D. Revier, and J. I. Lipton, "Expanding the design space for electrically-driven soft robots through handed shearing auxetics," in *2022 International Conference on Robotics and Automation (ICRA)*, 2022, pp. 10 951–10 957.

[27] I. Good, S. Balaji, and J. I. Lipton, "Torsion resistant strain limiting layers enable high grip strength of electrically-driven handed shearing auxetic grippers," 2024, arXiv:2412.07976.

VI. Biography Section



Xiaoqian Zhang Xiaoqian Zhang received the M.Eng. degree in Industrial Design Engineering from Guangdong University of Technology, China, in 2019. He is currently a doctoral candidate in Mechanical Engineering jointly supervised between the University of Genoa, Italy, and the Technical University of Munich, Germany. Before joining his doctoral program, he was a full-time Research Assistant at the Shenzhen Institutes of Advanced Technology, Chinese Academy of Sciences. His current research focuses on the mechanisms and control development of the soft and compliant robotic prosthetics, and grippers.



Mario Baggetta received his M.Sc., and Ph.D. degrees in Mechanical Engineering from the University of Genova in 2019, and 2023, respectively. Following his doctoral studies, he held postdoctoral positions at the University of Bologna and the University of Naples "Federico II". Currently, he is an Assistant Professor at the Department of Mechanical, Energy, Management and Transportation Engineering, University of Genova. His research interests include the integrated design of compliant mechanisms, variable stiffness actuators, cable-driven systems, and robotic hands for manipulation and prosthetics. He is actively involved in several research projects, including the FISA 2023 COMPANION project on compliant components for robotic manipulation and the HE IntelliMan project, which aims to develop an AI-based manipulation system for advanced robotic services and prosthetics.



Cristina Piazza Cristina Piazza received a B.Sc. in Biomedical Engineering, a M.S. in Automation and Robotics Engineering and a PhD degree in Robotics (summa cum laude, 2019) from the University of Pisa (Italy). She subsequently moved to Chicago (USA) where she worked as a postdoctoral researcher at Northwestern University. Since 2020, Prof. Piazza is tenure track assistant professor at Technical University of Munich. She is IEEE Senior Member and has received numerous awards for her scientific work, including the IEEE/RAS Early Career Award (2026), and the Kevin P. Granata Award (2026). Her main research interests include the study of human movement and the design of artificial devices based on soft robotics technologies for robotic and prosthetic applications.



Giovanni Berselli is Full Professor and Chair of Design Methods for Industrial Engineering at the University of Genova, Italy, where he coordinates the PhD Degree in Mechanical, Energy and Management Engineering. He is also Affiliated Researcher with the Advanced Robotics Department at the Italian Institute of Technology (IIT). Prof. Berselli is IEEE Senior Member, a Fellow of the ASME, the Chair of ASME – Italy Section, and the past Chair of the ASME Technical Committee on Modeling, Dynamics, and Control of Adaptive Systems. He has held Excellence Fellowships at TUM, DLR, KIT and visiting professor poistion and Harvard, MIT, MGH, UTwente and University of Navarra. Prof. Berselli's scientific activity is focused on the design, modelling and experimental evaluation of: i) robot hands and grippers; ii) compliant mechanisms and soft actuators for safe human-robot interaction; iii) energy-aware industrial robotics.